



**HAL**  
open science

# Investigation of Phase Segregation Dynamics in Ge-Rich GST Thin Films by In Situ X-Ray Fluorescence Mapping

Thomas Fernandes, Michael Texier, Philipp Hans, Cristian Mocuta, Solène Comby-dassonneville, Gabriele Navarro, Simon Jeannot, Thomas W Cornelius, Madeleine Han, Jaime Segura Ruiz, et al.

## ► To cite this version:

Thomas Fernandes, Michael Texier, Philipp Hans, Cristian Mocuta, Solène Comby-dassonneville, et al.. Investigation of Phase Segregation Dynamics in Ge-Rich GST Thin Films by In Situ X-Ray Fluorescence Mapping. *physica status solidi (RRL) - Rapid Research Letters (pss RRL)*, 2024, pp.2300408. 10.1002/pssr.202300408. hal-04733941

**HAL Id: hal-04733941**

**<https://hal.science/hal-04733941v1>**

Submitted on 13 Oct 2024

**HAL** is a multi-disciplinary open access archive for the deposit and dissemination of scientific research documents, whether they are published or not. The documents may come from teaching and research institutions in France or abroad, or from public or private research centers.

L'archive ouverte pluridisciplinaire **HAL**, est destinée au dépôt et à la diffusion de documents scientifiques de niveau recherche, publiés ou non, émanant des établissements d'enseignement et de recherche français ou étrangers, des laboratoires publics ou privés.



Distributed under a Creative Commons Attribution - NonCommercial 4.0 International License

# Investigation of Phase Segregation Dynamics in Ge-Rich GST Thin Films by In Situ X-Ray Fluorescence Mapping

Thomas Fernandes,\* Michael Texier, Philipp Hans, Cristian Mocuta, Solène Comby-Dassonneville, Gabriele Navarro, Simon Jeannot, Thomas W. Cornelius, Madeleine Han, Jaime Segura Ruiz, Martin Rosenthal, Yannick le Fric, Roberto Simola, and Olivier Thomas

Ge-rich Ge–Sb–Te alloy is a good candidate for future automotive applications due to its high crystallization temperature, which allows good data retention at elevated temperatures. Crystallization in this material is governed by elemental segregation which is key to thermal stability and device performance. In this work, elemental (Ge, Sb, Te) segregation is studied in situ during thermal annealing of Ge-rich Ge–Sb–Te thin films using X-ray fluorescence microscopy at ID16B beamline of ESRF with a beam size of 50 nm. Spatially resolved maps of Ge, Te, and Sb fluorescence yield are monitored and statistically analyzed as a function of temperature/time. In all investigated samples Sb appears to segregate much less than Te and Ge, indicating a lower mobility of this element. In situ, fluorescence mapping of samples doped with different amounts of carbon by ion implantation shows that carbon delays Ge and Te segregation to higher temperatures. Comparison with crystallization kinetics monitored by X-ray diffraction shows a good correlation between the occurrence of spatially resolved chemical inhomogeneities and the appearance of crystallized phases.

differences in their physical properties (resistivity, optical reflectivity, etc.) allow the state of the memory to be modified and read out. The most studied PCM is the ternary compound  $\text{Ge}_2\text{Sb}_2\text{Te}_5$  (called GST in literature), which has a crystallization temperature of 150–170 °C. However, this temperature is too low for data storage in many applications such as automotive. Ge-rich GST (GGST), in contrast, has a crystallization temperature of 350 °C,<sup>[5]</sup> making it an excellent candidate for embedded memory applications.<sup>[6]</sup> In previous work on N-doped GGST thin films, a sequential crystallization process was observed<sup>[7]</sup> based on synchrotron X-ray diffraction (XRD) measurements during thermal annealing (2 °C min<sup>-1</sup>). Ge was observed to crystallize before GST, indicating a phase separation. Hence, crystallization of GGST is related to spatial separation


## 1. Introduction

Phase change materials (PCMs) are very promising candidates for future nonvolatile memory applications.<sup>[1–4]</sup> The easy switching between the two phases (amorphous and crystalline) and the

of chemical elements, which directly influences the thermal stability and also affects PCM's endurance.<sup>[8]</sup> Reducing the germanium segregation can then improve the performance of the PCM in a number of ways, and there are several parameters that can be used to achieve this. The first option is to modify the composition

T. Fernandes, M. Texier, P. Hans, S. Comby-Dassonneville,  
T. W. Cornelius, O. Thomas  
Aix Marseille University  
University of Toulon  
CNRS, IM2NP UMR 7334  
13013 Marseille, France  
E-mail: thomas.fernandes@univ-amu.fr

T. Fernandes, S. Jeannot, Y. le Fric  
STMicroelectronics  
850 rue Jean Monnet, 38920 Crolles, France

 The ORCID identification number(s) for the author(s) of this article can be found under <https://doi.org/10.1002/pssr.202300408>.

© 2024 The Authors. physica status solidi (RRL) Rapid Research Letters published by Wiley-VCH GmbH. This is an open access article under the terms of the Creative Commons Attribution-NonCommercial License, which permits use, distribution and reproduction in any medium, provided the original work is properly cited and is not used for commercial purposes.

DOI: 10.1002/pssr.202300408

C. Mocuta  
Synchrotron SOLEIL  
l'Orme des Merisiers  
Saint-Aubin-BP 48, 91192 Gif-sur-Yvette, France

G. Navarro  
CEA LETI  
University Grenoble Alpes  
38000 Grenoble, France

M. Han, J. S. Ruiz, M. Rosenthal  
ID16B/ESRF, The European Synchrotron  
71 rue des Martyrs, 38043 Grenoble, France

M. Rosenthal  
DUBBLE/ESRF, The European Synchrotron  
71 rue des Martyrs, 38043 Grenoble, France

R. Simola  
STMicroelectronics  
190 Ave Coq, 13106 Rousset, France

of the underlayer (the layer under the Ge-rich GST film), as it directly affects the Ge-rich GST crystallization mechanisms. Doping (N, C, O, etc.) the GGST has also a strong influence on the segregation process<sup>[9]</sup> through the preferential bonding of the dopant with Ge, leading to an improved durability of

the PCM. This study will focus on the effect of doping on elemental segregation. The aim of the present study was to investigate phase separation in a spatially resolved manner using X-ray fluorescence (XRF) microscopy on a synchrotron beamline. We first describe the experimental method developed at ID16B-ESRF beamline. Maps of fluorescence yield for the three elements (Ge, Sb, Te) are measured in situ as a function of temperature or time. A statistical treatment of these maps is developed to quantify the element-dependent evolution of segregation. This strategy is applied to GGST thin films with different levels of carbon doping and the obtained results are compared with similar studies in the literature.<sup>[10]</sup>

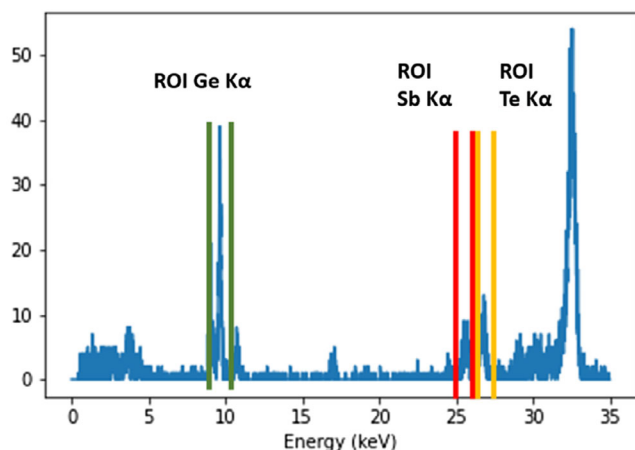


**Figure 1.** Typical XRF spectrum recorded with a 33 keV nanobeam ( $60 \text{ nm} \times 80 \text{ nm}$ ) on a 45 nm GGST film. Characteristic fluorescence lines for Ge, Sb, and Te are highlighted.

## 2. Results and Discussion

**Figure 1** shows an XRF spectrum with the contributions of Ge, Sb, and Te highlighted. By scanning the sample under the beam, it is possible to record  $(x,y)$  maps where each of the points contains a complete spectrum. The raw spectra are first normalized to the incident intensity monitored by the diode placed directly in front of the sample. In the second step, background fitting and subtraction followed by the numerical integration of the XRF peaks within the relevant region of interest, were performed, depending on the species selected. These regions of interest

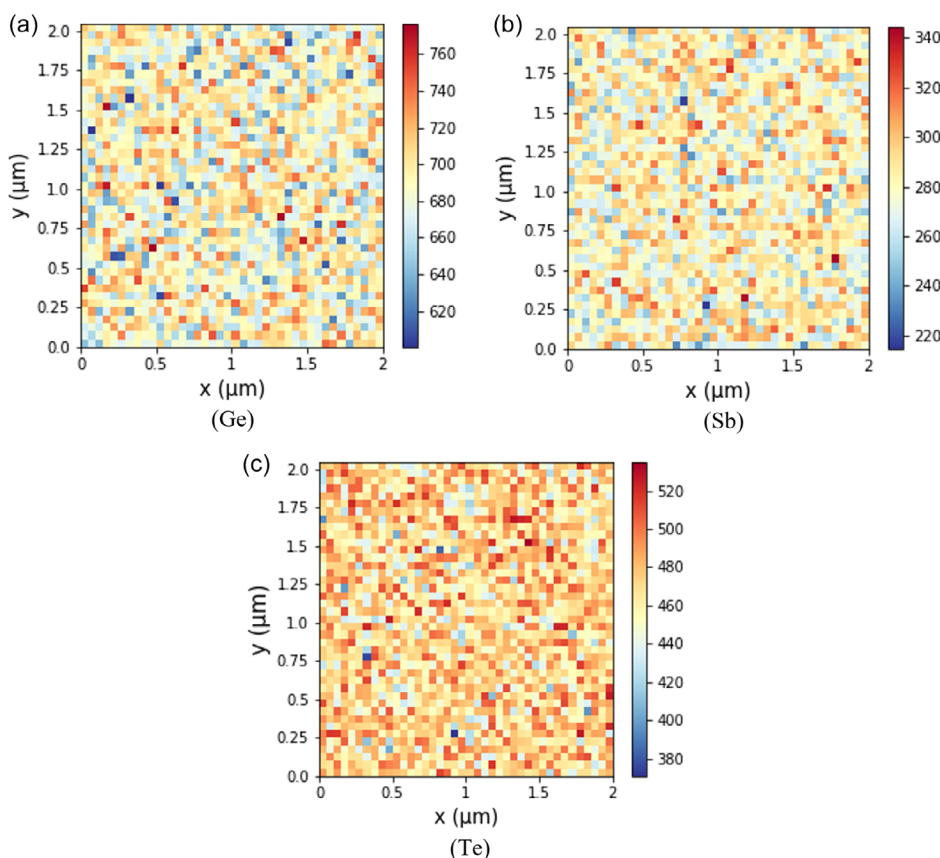


**Figure 2.** a) Fluorescence maps of germanium, b) antimony, and tellurium c) on a carbon-doped (C2) sample annealed at  $200 \text{ }^\circ\text{C}$  with a 33 keV nanobeam ( $60 \text{ nm} \times 80 \text{ nm}$ ). The maps are  $2 \text{ } \mu\text{m} \times 2 \text{ } \mu\text{m}$  with a step of 50 nm and a counting time of 30 ms. The color bar on the right-hand side corresponds to the fluorescence intensities.

are shown in Figure 1 with color bars and represent the area surrounding the fluorescence line of the element of interest. The germanium  $K\alpha$  is roughly in the range of 9.5 to 10.20 keV, the antimony  $K\alpha$  of 26 to 26.50 keV, and finally the tellurium  $K\alpha$  is in the range of 27 to 27.8 keV.

The resulting, pixelwise Ge, Sb, and Te fluorescence intensities are shown in Figure 2 and 3 in the form of  $(x,y)$  maps. Each fluorescence map in Figure 2 and 3 is  $2\ \mu\text{m} \times 2\ \mu\text{m}$  with a step of 50 nm and a count time of 30 ms. While Ge  $K\alpha$ , Te  $K\alpha$ , and Sb  $K\alpha$  maps show spatially homogeneous fluorescence yields in pristine samples, as in Figure 2, clear variations appear after annealing at 420 °C, as shown in the fluorescence maps in Figure 3, indicating elemental segregation. Furthermore, in the annealed state, Ge-rich areas correlate with Te-poor areas and Sb-poor areas.

To study the segregation of the three elements in a more quantitative way, histograms of the Ge, Sb, and Te yields were extracted from each map. By analyzing the moments of these distributions as a function of temperature or time, it is possible to characterize the kinetics of Ge, Sb, and Te segregation. As shown in Figure 4, the histogram is strongly influenced by the elemental segregation: after annealing at 420 °C, the conditions yielding a highly segregated sample (Figure 3b) show a histogram of the Ge distribution that is spread out on the left-hand side. The histograms shown in Figure 4 have 50 intensity bins, the intensity range for each bin in Figure 4a is 3.53 a.u., in Figure 4b, it is 4.46 a.u., in Figure 4c, it is 2.6 a.u., in Figure 4d, it is 3.04 a.u.,

in Figure 4e, 3.29 a.u., and in Figure 4f, it is 5.84 a.u. This dispersion of the histogram can be easily quantified by the standard deviation  $\sigma$  of the distribution which is considered as an indicator of the elemental segregation. In the following,  $\sigma$  is the parameter chosen to monitor the temperature (or time) evolution of Ge, Te, and Sb segregation. To successfully extract the standard deviation from the fluorescence maps, the Numpy library<sup>[11]</sup> was used as it contains functions well suited for calculating standard deviations for arrays.

To evaluate the influence of carbon doping on elemental segregation, we conducted in situ XRF mapping experiments during annealing on a product of reference sample (POR, no C-doping) and two C-doped samples (C1 and C2: C1 [E keV, D  $\text{cm}^{-2}$ ], C2[0.6\*E keV, D/4  $\text{cm}^{-2}$ ]). Figure 5 shows the standard deviations for germanium, tellurium, and antimony as a function of temperature (from 300 °C to 420 °C at  $2\ \text{C min}^{-1}$ ) and helps to understand the dynamics of elemental segregation. For the POR sample, the behavior of Te and Ge is similar. However, for the two doped samples, germanium tends to segregate less than tellurium. Above an approximate temperature of 380 °C (POR), 390 °C (C1), or 350 °C (C2), there is a rapid increase in the standard deviation, which is the signature of an increasing elemental segregation with the annealing temperature. Furthermore, the trend for all samples indicates that Te segregation is stronger than Ge segregation when carbon doping is present. Interestingly, the observed Ge and Te segregation contrasts

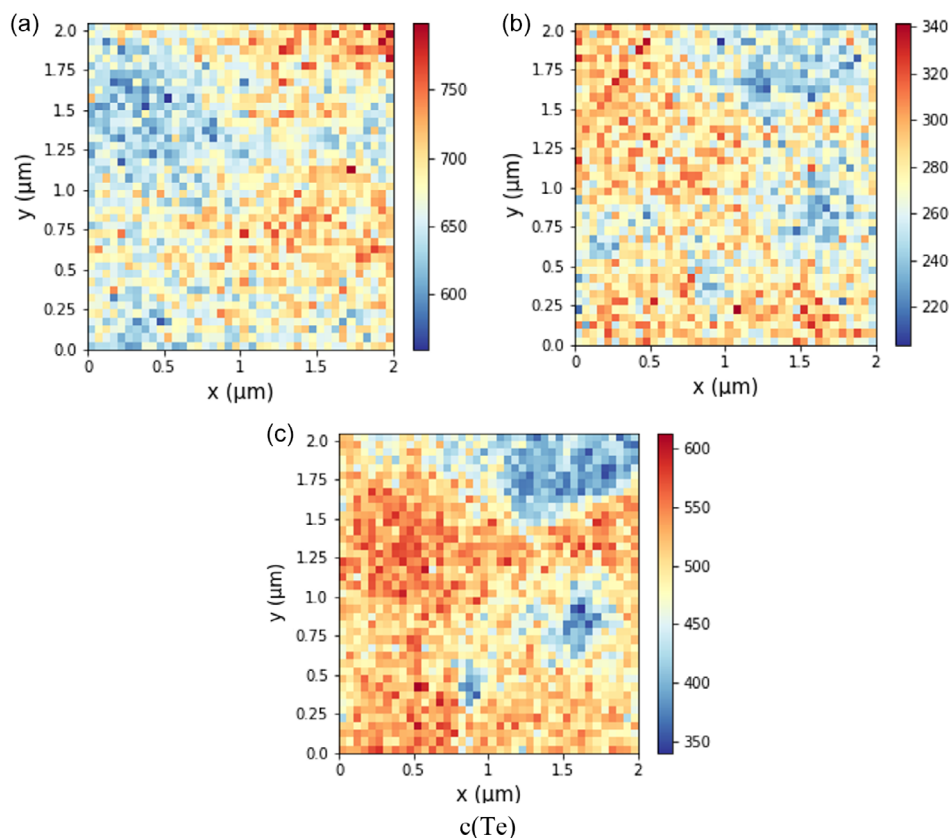


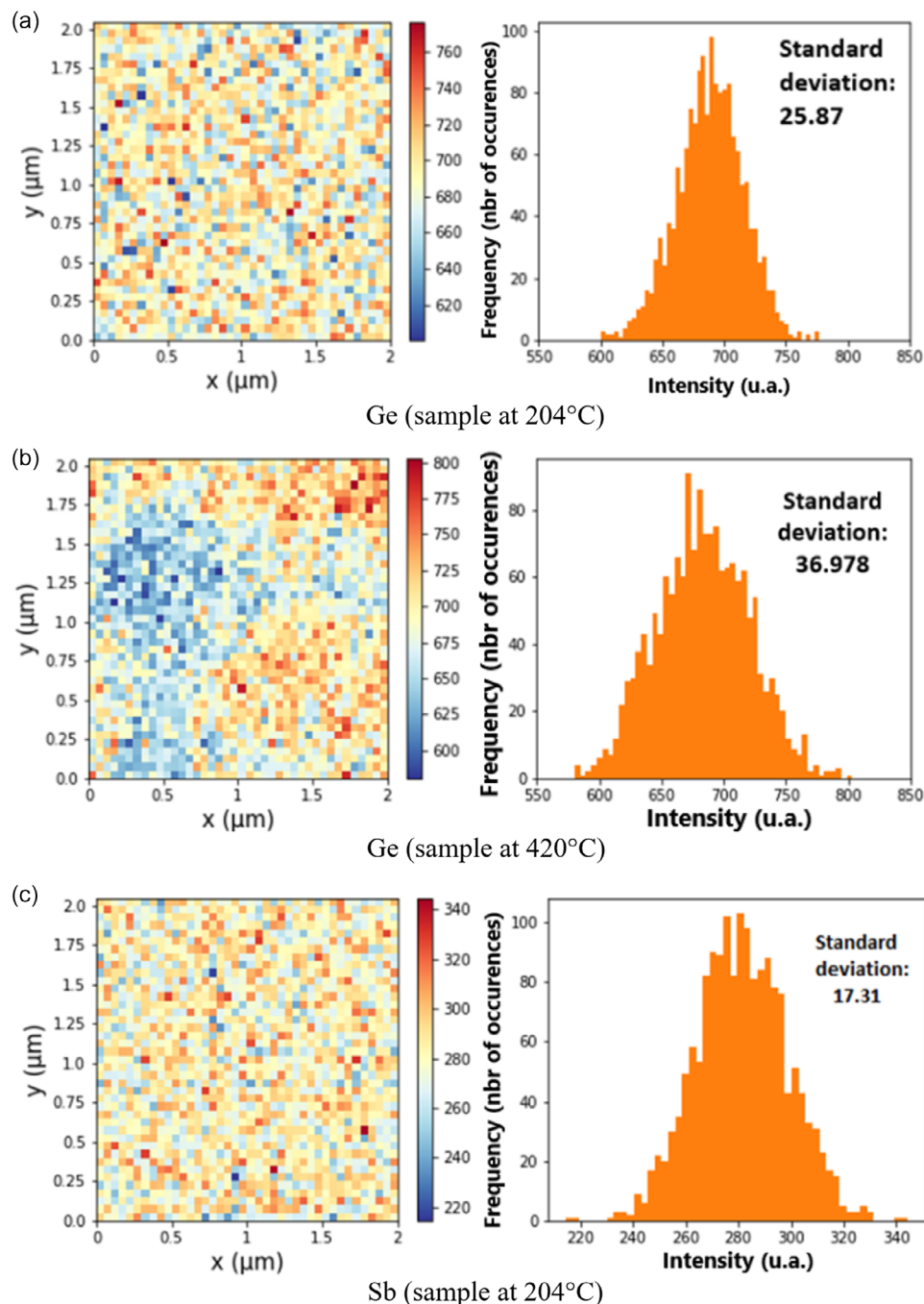
**Figure 3.** a) Fluorescence maps of germanium, b) antimony, and c) tellurium on a carbon-doped (C2) sample annealed at 420 °C with a 33 keV nanobeam ( $60\ \text{nm} \times 80\ \text{nm}$ ). The maps are  $2\ \mu\text{m} \times 2\ \mu\text{m}$  with a step of 50 nm and a counting time of 30 ms. The color bar on the right-hand side corresponds to the fluorescence intensities.

with the absence of significant Sb segregation. This low Sb mobility is surprising given its low melting point, but it is consistent with recent findings on the diffusion of Ge, Te, and Sb in GST.<sup>[12]</sup> Similarly, the observed mobility hierarchy (Te>Ge>Sb) is consistent with published works.<sup>[12]</sup>

As a continuation of the ramp anneal, the temperature was maintained at 420 °C for a duration of 30 to 70 min depending

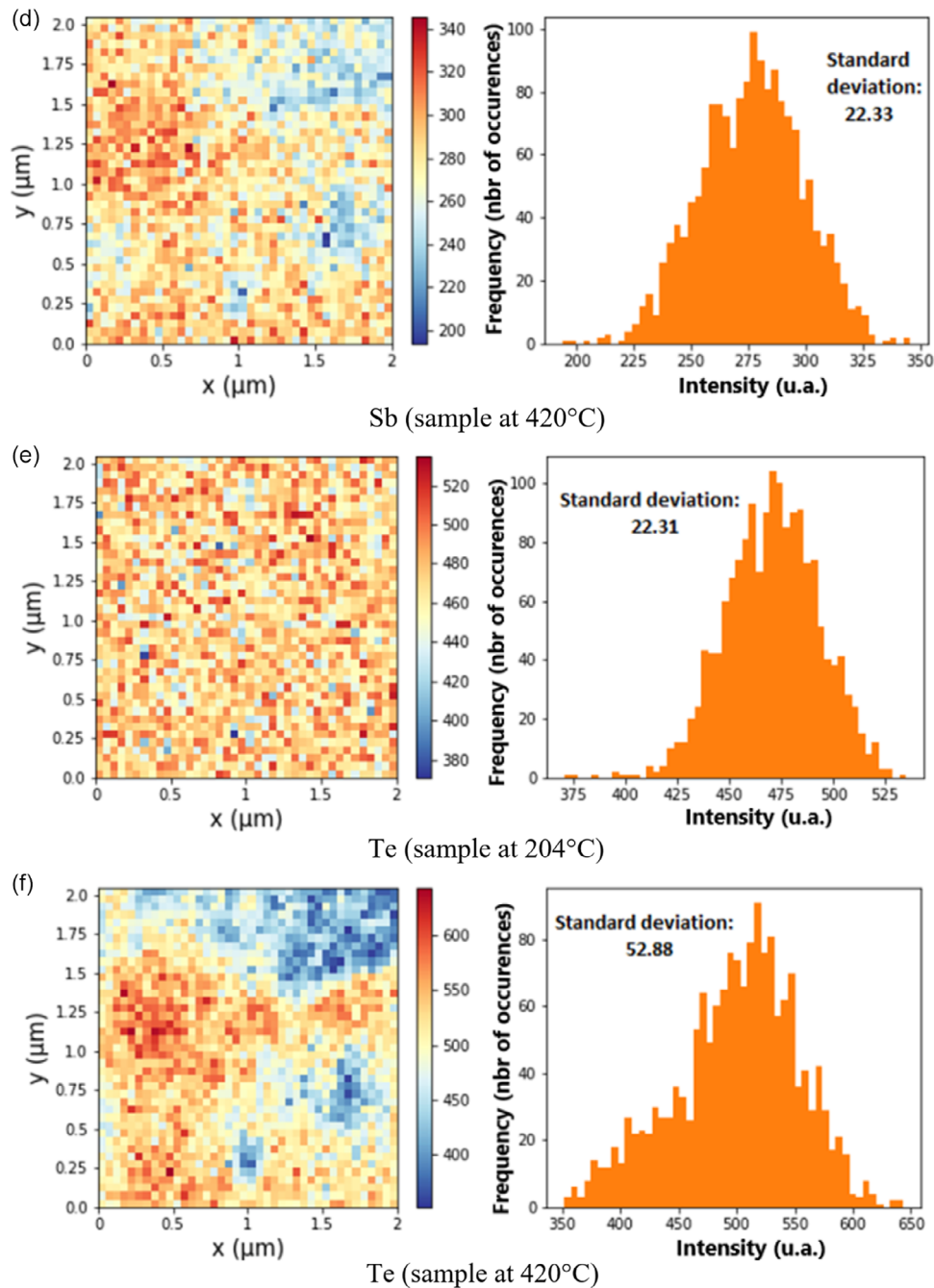
on the sample. The standard deviations of each element were then plotted as a function of time, here against each sample for each element, as the system is already highly segregated this helps to compare the effect of carbon doping on segregation. (Figure 6).

Figure 6 shows that the samples are already highly segregated. This explains why the dynamics of elemental segregation is low.



**Figure 4.** a) Fluorescence maps of germanium in a carbon-doped C2 sample at 204 °C and b) 420 °C, c) antimony C2 sample at 204 °C and d) 420 °C, and e) tellurium C2 sample at 204 °C and f) 420 °C with a 33 keV nanobeam (60 nm × 80 nm). The maps are 2 μm × 2 μm with a step of 50 nm and a counting time of 30 ms. The color bar on the right-hand side corresponds to the fluorescence intensities. The histograms are associated with the distribution of fluorescence intensities.





**Figure 4.** Continued.

It is observed that Te segregates faster than Ge and Sb. The non-doped POR sample exhibits the highest level of segregation. On the contrary, carbon doping reduces segregation, this inhibitory effect possibly being caused by the preferential C–Ge bonding shown by photoelectron spectroscopy in C-doped GST samples.<sup>[10]</sup>

In situ XRD experiments previously performed on the DiffAbs-SOLEIL beamline<sup>[7]</sup> allowed the intensity of the Ge 111 and GST 200 diffraction peaks to be monitored as a function of time during isothermal annealing (see **Figure 7** for an

isothermal anneal on a 50 nm GGST film with no underlayer). Assuming no evolution of the crystallographic texture, this integrated intensity is proportional to the volume of crystallized Ge or GST in the film. The occurrence of pure Ge crystallization from a Ge–Sb–Te film implies elemental segregation, and it has been shown that this segregation occurs prior to Ge crystallization.<sup>[13]</sup> To demonstrate this phase separation and compare it with the crystallization evolution, we used XRF mapping on samples annealed under exactly the same conditions (same furnace used for the preannealed samples as for XRD samples) as in

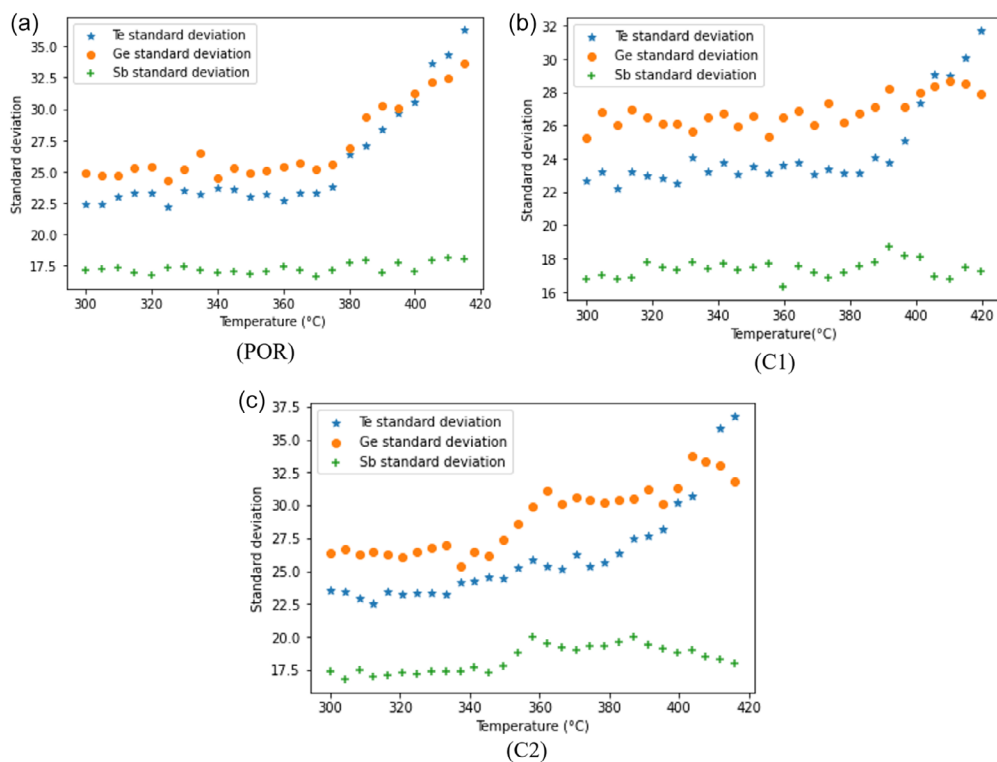


**Figure 5.** a) Evolution of the standard deviation of POR, b) C1, and c) C2 fluorescence intensity distributions acquired during in situ heating experiments between 300 °C and 420 °C with the three elements.

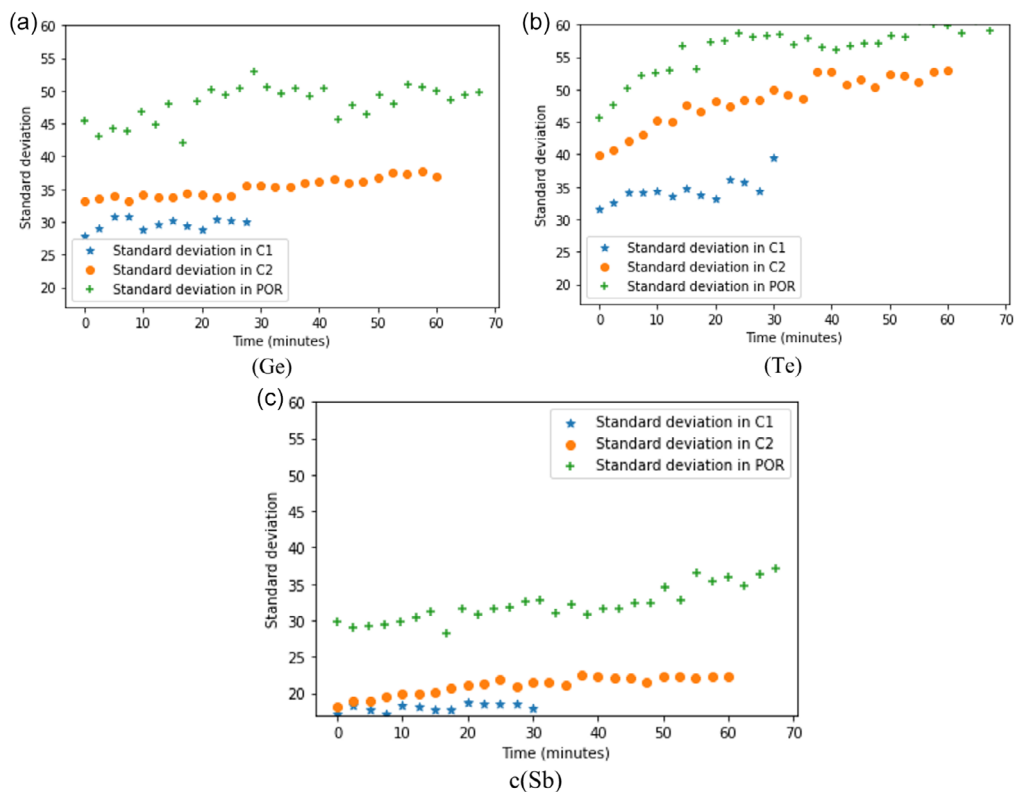


**Figure 6.** a) Standard deviation of Ge, b) Te, and c) Sb fluorescence intensity distributions acquired during in situ isothermal heating at 420 °C with different carbon doping conditions.

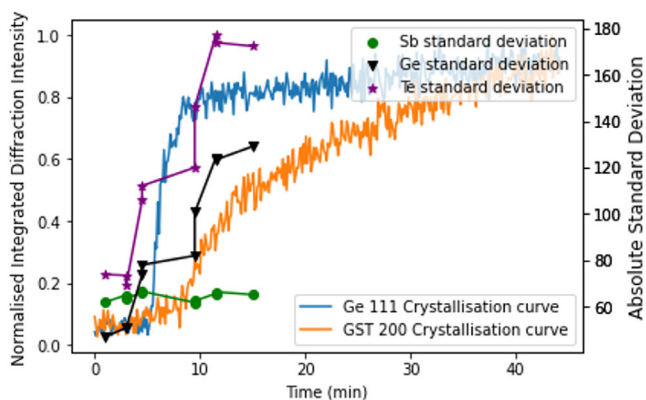


**Figure 7.** Standard deviation values for the germanium, antimony, and tellurium (plotted respectively as triangles, dots, and stars) from GGST superimposed to the Ge 111 and GST 200 crystallization curves performed for an isothermal anneal at 420 °C (plotted as solid lines) as a function of the isothermal annealing time (in minutes).

DiffAbs and quenched after selected times. To compare in situ XRD and ex situ XRF data, the same data treatment was applied to each fluorescence map: the distribution moments were extracted from the intensity histograms. For the ex situ experiments, the fluorescence maps have a size of  $4 \times 4 \mu\text{m}^2$ , with 40 nm steps and 100 ms exposure time.

Figure 7 shows the standard deviation for germanium, tellurium, and antimony measured from XRF maps, superimposed with the evolution of the integrated intensity of Ge 111 and GST 200 as a function of the annealing time. The standard deviation values are not normalized to allow for a comparison between each element. Overall, there is a good agreement between the evolution of the Ge crystallized fraction and the evolution of the germanium and tellurium standard deviation from the XRD maps. However, it is clear that antimony has a low mobility as the standard deviation does not appear to evolve with time. The agreement between XRF and XRD data confirms that Ge crystallization in the Ge–Sb–Te alloy is accompanied by elemental segregation. In contrast, it is difficult to conclude elemental segregation in the amorphous state (for annealing times below 4 min) due to the scatter in the measurements. This dispersion is partly due to the difficulty of obtaining exactly the same annealing conditions for such short times between quenched samples and samples observed in situ during annealing. To avoid this problem, XRF and XRD experiments should be performed at the same time in situ.

### 3. Conclusion

In conclusion, this study reports the results obtained from in situ XRF experiments performed on carbon-doped GGST samples to observe the effect of carbon doping on elemental segregation in a Ge-rich Ge–Sb–Te alloy. Elemental maps were recorded as a function of temperature or time using the intense and highly focused X-ray beams available at ID16B (ESRF). The following conclusions can be drawn: 1) In situ XRF microscopy appears as a suitable technique for in situ investigating elemental segregation over large areas in thin chalcogenide films during thermal

annealing. A complete methodology has been developed, including sample preparation and data treatment. 2) The segregation dynamics of the three elements that constitute GGST appear to differ. Segregation of Te is predominant, while no significant segregation of Sb is evidenced until about 420 °C. These features agree with the results reported in a recent study of the diffusion of chemical species in  $\text{Ge}_2\text{Sb}_2\text{Te}_5$ .<sup>[12]</sup> 3) Carbon slows down the segregation of elements, particularly Ge. This may explain the beneficial influence of C on the electrical properties of memory devices. 4) The elemental segregation measured using XRF microscopy has been compared with the crystallization kinetics showed by the evolution of XRD integrated intensities on the same samples. An overall agreement between the trends given by the two techniques is obtained. XRF maps indicate that germanium and tellurium have the same segregation dynamics, even in noncarbon-doped Ge-rich GST samples, and that antimony shows little to no mobility. However, it remains unclear whether elemental segregation occurs in the amorphous phase before Ge or GST crystallization. To obtain such information, XRD and XRF should be carried out simultaneously in situ.

### 4. Experimental Section

The XRF experiments were performed on the ID16B beamline at the ESRF (France). The incident X-ray beam was focused down to  $60 \times 80 \text{ nm}^2$  using KB mirrors and an incident photon energy of 33 keV was chosen to excite the Ge  $K\alpha$ , Sb  $K\alpha$ , and Te  $K\alpha$  fluorescence lines. Two silicon drift detectors were used for this experiment and positioned in the horizontal plane at 15° with respect to the sample surface, the two detectors used in this experiment form a total active area of 400 mm<sup>2</sup> and 350 μm thickness. A piezoelectric stage (90 μm of total range) allows the sample to be moved in front of the beam with a resolution of 37 nm allowing scanning XRF microscopy to be performed. The samples investigated include 45 nm thick GGST thin films embedded in the following stacks: Si (001) substrate//30 nm SiO<sub>2</sub>//75 nm Si<sub>3</sub>N<sub>4</sub>//5 nm UL//45 nm GGST (C-doped)//20 nm TiN//25 nm Si<sub>3</sub>N<sub>4</sub>, where UL stands for Ge<sub>2</sub>Sb<sub>2</sub>Te<sub>5</sub> underlayer. GGST layers are deposited by physical vapor deposition (PVD) followed by an in situ PVD TiN capping using an industrial dedicated setup. The SiN capping is then deposited by chemical vapor deposition. The capping layers ensure that the GGST films are protected against oxidation. Carbon doping is achieved by ion implantation. In this work, two different C doping levels were investigated, varying the implantation energy (E) and the implanted dose (D): C1 [E keV, D cm<sup>-2</sup>], C2 [0.6\*E keV, D/4 cm<sup>-2</sup>]. Samples were annealed in situ using a microheater-based furnace developed at ESRF.<sup>[14]</sup> XRF maps were monitored in situ during ramp annealing from 200 °C to 420 °C at a heating rate of 2 °C min<sup>-1</sup>. Isothermal anneals at 420 °C were also performed. To fit on the microheater and to reduce the thermal mass, samples with lateral dimensions of 30 × 30 μm<sup>2</sup> and a height of 15–20 μm were prepared either by FIB micromachining or by mechanical polishing and cleaving. In addition to the in situ measurements, fluorescence maps were also recorded on Ge-rich GST samples, without underlayer and without carbon doping. These samples were preannealed at the DiffAbs SOLEIL synchrotron beamline under exactly the same conditions (furnace, temperature, time) as used for the in situ XRD measurements.<sup>[15]</sup>

### Acknowledgements

The authors gratefully acknowledge ESRF and SOLEIL for allocating beam time. OT acknowledges the support of Ennio Caprio (ESRF) and IRT Nanoelec for providing the first beamtime that allowed demonstrating the feasibility of the experiment. This research was supported by IPCEI/Nano 2022 program.



## Conflict of Interest

The authors declare no conflict of interest.

## Data Availability Statement

The data that support the findings of this study are available from the corresponding author upon reasonable request.

## Keywords

GST, nonvolatile memories, phase change materials, synchrotron radiation, X-ray fluorescence imaging

Received: October 30, 2023

Revised: February 26, 2024

Published online:

- 
- [1] H. S. P. Wong, S. Raoux, S. Kim, J. Liang, J. P. Reifenberg, B. Rajendran, M. Asheghi, K. E. Goodson, *Proc. IEEE* **2010**, *98*, 2201.
- [2] R. F. Freitas, W. W. Wilcke, *IBM J. Res. Dev.* **2008**, *52*, 439.
- [3] G. W. Burr, B. N. Kurdi, J. C. Scott, C. H. Lam, K. Gopalakrishnan, R. S. Shenoy, *IBM J. Res. Dev.* **2008**, *52*, 449.
- [4] D. J. Wouters, R. Waser, M. Wuttig, *Proc. IEEE* **2015**, *103*, 1274
- [5] P. Zuliani, E. Palumbo, M. Borghi, G. Dalla Libera, R. Annunziata, *Solid State Electron* **2015**, *111*, 27.
- [6] F. Arnaud, P. Ferreira, F. Piazza, A. Gandolfo, P. Zuliani, P. Mattavelli, E. Gomiero, G. Sammanni, J. Jasse, C. Jahan, J. P. Reynard, R. Berthelon, O. Weber, A. Villaret, B. Dumont, J. C. Grenier, R. Ranica, C. Gallon, C. Boccacio, A. Souhaite, L. Desvoivres, D. Ristoiu, L. Favennec, V. Caubet, S. Delmedico, N. Cherault, R. Beneyto, S. Chouteau, P. O. Sassoulas, L. Clement, et al., in *IEEE Int. Electron Devices Meeting IED*, San Francisco, CA, December **2020**, pp. 24.2.1–24.2.4.
- [7] O. Thomas, C. Mocuta, M. Putero, M.-I. Richard, P. Boivin, F. Arnaud, *Microel. Eng.* **2021**, *244–246*, 111573.
- [8] Y. H. Lee, P. J. Liao, V. Hou, D. Heh, C. H. Nien, W. H. Kuo, G. T. Chen, S. M. Yu, Y. S. Chen, J. Y. Wu, X. Bao, C. H. Diaz, in *IEEE Int. Reliability Physics Symp. IRPS*, Monterey, CA, March **2021**, <https://doi.org/10.1109/irps46558.2021.9405168>.
- [9] L. Prazakova, E. Nolot, E. Martinez, F. Fillot, D. Rouchon, N. Rochat, M. Bernard, C. Sabbione, D. Morel, N. Bernier, A. Grenier, A.-M. Papon, M.-C. Cyrille, G. Navarro, *J. Appl. Phys.* **2020**, *128*, 215102.
- [10] M. C. Jung, Y. Lee, K. Kim, *Curr. Appl. Phys.* **2014**, *14*, 1421.
- [11] C. R. Harris, K. J. Millman, S. J. Van Der Walt, R. Gommers, P. Virtanen, D. Cournapeau, E. Wieser, J. Taylor, S. Berg, N. J. Smith, R. Kern, M. Picus, S. Hoyer, M. H. Van Kerkwijk, M. Brett, A. Haldane, J. F. Del Río, M. Wiebe, P. Peterson, P. Gérard-Marchant, K. Sheppard, T. Reddy, W. Weckesser, H. Abbasi, C. Gohlke, T. E. Oliphant, *Nature* **2020**, *585*, 357.
- [12] M. Anh Luong, S. Ran, C. Sabbione, A. Claverie, *Mater. Sci. Semicond. Process.* **2023**, *164*, 107644.
- [13] M. Rosenthal, D. Doblas, J. J. Hernandez, Y. I. Odarchenko, M. Burghammer, E. Di Cola, D. Spitzer, A. E. Antipov, L. S. Aldoshin, D. A. Ivanov, *J. Synch. Rad.* **2014**, *21*, 223.
- [14] M. Agati, M. Vallet, S. Joulié, D. Benoit, A. Claverie, *J. Mater. Chem. C* **2019**, *7*, 8720.
- [15] P. Hans, C. Mocuta, Y. Le-Friec, P. Boivin, R. Simola, O. Thomas, *J. Appl. Phys.* **2023**, *134*, 105102.